JOURNAL OF NEUROTRAUMA 31:938–950 (May 15, 2014)

DOI: 10.1089/neu.2013.3144

# Diffusion Tensor Imaging Reveals White Matter Injury in a Rat Model of Repetitive Blast-Induced Traumatic Brain Injury

Evan Calabrese,[1] Fu Du,[2] Robert H. Garman,[3] G. Allan Johnson,[1] Cory Riccio,[4] Lawrence C. Tong,[4] and Joseph B. Long[4]

## Abstract

Blast-induced traumatic brain injury (bTBI) is one of the most common combat-related injuries seen in U.S. military personnel, yet relatively little is known about the underlying mechanisms of injury. In particular, the effects of the primary blast pressure wave are poorly understood. Animal models have proven invaluable for the study of primary bTBI, because it rarely occurs in isolation in human subjects. Even less is known about the effects of repeated primary blast wave exposure, but existing data suggest cumulative increases in brain damage with a second blast. MRI and, in particular, diffusion tensor imaging (DTI), have become important tools for assessing bTBI in both clinical and preclinical settings. Computational statistical methods such as voxelwise analysis have shown promise in localizing and quantifying bTBI throughout the brain. In this study, we use voxelwise analysis of DTI to quantify white matter injury in a rat model of repetitive primary blast exposure. Our results show a significant increase in microstructural damage with a second blast exposure, suggesting that primary bTBI may sensitize the brain to subsequent injury.

**Key words:** blast neurotrauma; diffusion tensor imaging; MRI; traumatic brain injury; voxelwise analysis

## Introduction

Blast-induced traumatic brain injury (bTBI) is one of the most common injuries seen in U.S. military personnel returning from Iraq and Afghanistan. Although exact numbers are difficult to calculate, the prevalence of bTBI has been estimated to be as high as 18% among U.S. combat veterans.[1] The nature of current military conflicts, as well as improvements in body armor and battlefield trauma care, have resulted in an increasing number of veterans with bTBI as their sole, persisting, combat-related morbidity.[2,3] These patients experience a wide range of subtle neurological symptoms including persistent headache, insomnia, vertigo, tinnitus, psychomotor agitation, and difficulty concentrating.[1] These symptoms are often extremely debilitating and can prevent veterans from returning to civilian employment after leaving active duty.[4] Unfortunately, relatively little is known about the exact mechanism of injury underlying bTBI, and there is currently no universally accepted standard for diagnosis, prognosis, or treatment of bTBI. Further, the long-term sequelae of bTBI are largely unknown, although it has been theorized that bTBI may contribute to a number of psychological diseases including post-traumatic stress disorder and other anxiety disorders.[4] These uncertainties surrounding bTBI highlight the need for a more rigorous understanding of the underlying mechanisms of injury.

There is considerable clinical overlap between bTBI and civilian TBI caused by acute blunt head trauma (e.g., from accidents) and/or repetitive low-impact blows to the head (e.g., from participation in full contact sports).[1,2,5–7] This has led many to assume that the underlying mechanisms of injury are the same; however, this simplistic view may overlook some of the fundamental physical differences between bTBI and civilian TBI. Blast-induced brain injury is often divided into several different mechanisms of injury, each of which likely contributes to the overall clinical syndrome associated with bTBI. The most commonly cited model divides bTBI into primary (the direct result of the propagating blast pressure wave), secondary (caused by shrapnel and debris accelerated by the explosion), and tertiary injury (a coup-countercoup injury caused by rapid acceleration and deceleration of the brain inside the neurocranium).[8] Of these mechanisms of injury, only primary bTBI differs significantly from the types of injury commonly seen in

[1]Center for In Vivo Microscopy, Department of Radiology, Duke University Medical Center, Durham, North Carolina.
[2]FD NeuroTechnologies, Inc., Ellicott City, Maryland.
[3]Safar Center for Resuscitation Research, University of Pittsburgh School of Medicine, Pittsburgh, Pennsylvania.
[4]Blast-Induced Neurotrauma Branch, Center for Military Psychiatry and Neuroscience, Walter Reed Army Institute of Research, Silver Spring, Maryland.

civilian TBI. There is considerable debate on what, if any, effect primary bTBI has on the injury as a whole. This debate stems from the fact that primary bTBI is rarely seen in isolation in clinical populations; however, the limited number of case reports that do exist suggest that primary bTBI may be a key difference between bTBI and civilian TBI.[9–11]

A number of recent animal studies have provided evidence indicating that primary bTBI may play an important role in both direct brain injury and in sensitization to further brain injury.[12–16] Animal models allow primary bTBI to be studied in isolation and, perhaps more importantly, allow a more comprehensive assessment of brain pathology than is possible in human subjects. In particular, compression driven shock tubes can provide a robust and reproducible simulation of primary blast overpressure in rats and mice.[12,15] The shock tube model can be used to study numerous aspects of primary bTBI including the scope, location, and time course of the associated brain injury. Interestingly, a small number of shock tube studies have shown that repeated exposure to blast overpressure causes significantly increased neuronal damage, suggesting a synergistic effect.[17–20] This has lead some to theorize that primary bTBI may be a key sensitization to subsequent brain injury.[6] Animal studies may be the single most important tool for understanding the fundamental differences between bTBI and civilian TBI, which will be essential for guiding treatments designed to prevent, mitigate, and treat the associated brain injury.

Light-microscopy–based histology is the current ''gold standard'' for assessing neuropathology in animal models of bTBI. Conventional histology has several important limitations in this application; first, it is destructive, and therefore pathology can only be assessed in a single plane; second, it is time-consuming and labor intensive, making whole-brain assessment impractical; third, light microscopy images are difficult to quantify because tissue volume is often altered during sectioning, and stain density is highly variable between specimens; finally, conventional histology is only possible in fixed, *ex vivo* tissue, and therefore is not translatable to clinical populations.

MRI-based microimaging techniques are emerging as a valuable alternative to conventional histology for assessing neuropathology in animal models.[21–23] Like conventional histology, MRI can be used to assess neuropathology on the microscopic scale; however, MRI has several key advantages[24]; it is non-destructive and can be performed with the brain *in situ* in the neurocranium; it can survey the entire brain in three dimensions with isotropic spatial resolution, allowing assessment in any arbitrary plane as well as in three dimensions; it is inherently digital, and many MRI contrasts are quantitative in nature; finally, small animal MRI data can be processed and analyzed using the same tools and methodology used in clinical MRI data, making results directly translatable to humans.[25]

Diffusion tensor imaging (DTI) is an MRI acquisition strategy that provides quantitative, brain-wide maps of water diffusion characteristics that reveal underlying tissue microstructure.[26] Several of these tissue microstructural parameters are useful for detecting neuropathology. For example, fractional anisotropy (FA) is sensitive to white matter integrity, and mean diffusivity (MD) is altered in necrosis, edema, and gliosis.[27] Importantly, there is a growing body of clinical data demonstrating the use of diffusion tensor parameters to quantify bTBI.[6,28] These studies show a range of bTBI-associated injuries that can be detected with DTI, particularly in major white matter tracts. For example, Sponheim and associates[28] and Mac Donald and colleagues[29] showed statistically significant decreases in anisotropy in several major white matter pathways of U.S. military personnel with bTBI, including the corpus callosum, and cerebellar peduncles. DTI has also been used to detect TBI in a number of small animal studies[12,30,31]; however, none of these studies have assessed the effects of repeated primary bTBI.

In this study, we use voxelwise analysis of diffusion tensor parameters to quantify brain microstructural changes in a rat model of repetitive bTBI. These data reveal dramatic differences in the microstructural brain damage caused by a single blast exposure and a tightly temporally coupled double blast exposure. We further validate our findings using conventional histology and show that changes in DTI microstructural metrics correlate with histological changes. The methods presented here allow quantitative assessment of primary bTBI in an animal model with clinically translatable image processing techniques. These data add to a growing body of data suggesting that blast overpressure contributes to bTBI associated brain injury and may be a key sensitization to subsequent brain injury.

## Methods

### *Animals and experimental design*

All experiments and procedures were performed with the approval of both the Walter Reid Army Institute of Research and the Duke University Institutional Animal Care and Use Committee. Adult, male Sprague-Dawley rats (250–300 g) were housed on a 12-h/12-h light/dark cycle and were provided access to standard rat chow *ad libitum*. Rats were randomized into three experimental groups of nine animals each: a sham control group, a single blast exposed group, and double blast exposed group. All three groups were deeply anesthetized in an induction box by breathing a 4% isoflurane mixture in air delivered at 2 L/min for 6 min. The sham control group was handled in an identical manner but was not exposed to blast overpressure. The single blast group was exposed to a single shockwave (18.3 PSI static pressure, 8.8 msec positive phase duration). The double blast group was exposed to two identical shockwaves separated temporally by 1 min. All three groups were given 72 h to recover from anesthesia and blast exposure before euthanasia and imaging experiments.

### *Air-blast exposure*

Air-blast exposure was generated using a 1-ft-diameter shock tube consisting of a 2.5-ft-long air compression chamber and a 15-ft-long expansion chamber separated by a Mylar membrane manufactured to rupture at a specific pressure. A high-volume air compressor was used to pressurize the compression chamber with room air until the Mylar membrane rupture pressure was reached. Flow conditions were recorded using piezoresistive pressure transducers (Meggit Inc., San Juan Capistrano, CA) mounted in the rat holder and provided measurements of total and side-on pressure waveforms. All rats were tautly secured in a transverse prone position in coarse mesh netting 2.5 ft within the mouth of the expansion chamber with the right side of the head facing the pressure chamber. Blast overpressure exposure was generally well tolerated; however, one rat in the double-blast group died shortly after blast exposure and was excluded from the analysis.

### *Specimen preparation for imaging experiments*

Animals were perfusion-fixed using the active staining technique described more completely by Johnson et al.[32] Perfusion fixation was achieved using a 10% solution of neutral buffered formalin (NBF) containing 10% (50 mM) gadoteridol (ProHance, Bracco Diagnostics, Milan, Italy). After perfusion fixation, rat heads were removed and immersed in 10% NBF for 24 h. Finally, fixed rat heads were transferred to a 0.1 M solution of phosphate

buffered saline containing 1% (5 mM) gadoteridol at 4°C for 5–7 days. Before imaging, specimens were placed in custom-made, MRI-compatible tubes and immersed in Fomblin® low viscosity perfluoropolyether (Ausimont USA, Thorofare, NJ) for susceptibility matching and to prevent specimen dehydration. All imaging experiments were performed with the brain in the neurocranium to preserve tissue integrity and native spatial relationships.

### *Image acquisition*

Imaging was performed on a 7 Tesla small animal MRI system (Magnex Scientific, Yarnton, Oxford, UK) equipped with 650 mT/m Resonance Research gradient coils (Resonance Research, Inc., Billerica, MA), and controlled with a General Electric Signa console (GE Medical Systems, Milwaukee, WI). RF transmission and reception was achieved using a custom 30 mm diameter × 50 mm long solenoid coil. T2*-weighted gradient recalled echo (GRE) anatomical images were acquired using a three-dimensional (3D) sequence (TR = 50 ms, TE = 8.3 ms, NEX = 2, $\alpha = 60$ degrees). The acquisition matrix was $1024 \times 512 \times 512$ over a $40 \times 20 \times 20$ mm field of view (FOV). The Nyquist isotropic spatial resolution was 39 $\mu$m.

Diffusion tensor data sets were acquired using a spin-echo pulse sequence (TR = 100 ms, TE = 16.2 ms, NEX = 1). Diffusion preparation was accomplished using a modified Stejskal-Tanner diffusion-encoding scheme[33] with a pair of unipolar, half-sine diffusion gradient waveforms (width $\delta = 4$ ms, separation $\Delta = 8.5$ ms, gradient amplitude = 450 mT/m). One b0 image and six high b-value images (b = 1500 s/mm$^2$) were acquired with diffusion sensitization along each of six non-colinear diffusion gradient vectors: (1, 1, 0), (0, 1, 1), (1, 0, 1), (1, −1, 0), (0, 1, −1), and (−1, 0, 1). The acquisition matrix was $512 \times 256 \times 256$ over a $40 \times 20 \times 20$ mm FOV. The Nyquist isotropic spatial resolution was 78 $\mu$m. All images were derived from fully sampled k-space data with no zero-filling. All images had a signal-to-noise-ratio (SNR) of 30 or greater.

### *DTI processing*

Diffusion data were processed with a custom image-processing pipeline that comprised freely available software packages including Perl (http://www.perl.org), ANTs (http://www.picsl.upenn.edu/ANTS/), and Diffusion Toolkit (http://www.trackvis.org). This automated pipeline was created to ensure that all data were processed in the same way and to reduce the potential for user error. First, diffusion-weighted image volumes were rigidly aligned to the b0 volume using ANTs to correct for the linear component of eddy current distortions. Next, diffusion tensor estimation and calculation of tensor-derived data sets were performed using Diffusion Toolkit (http://trackvis.org/dtk/). Finally, data were organized into a consistent file architecture and archived in NIfTI format (http://nifti.nimh.nih.gov) in an on-site Oracle database.[34]

### *Image registration and averaging*

Interspecimen registration of MR data was accomplished with the ANTs software package.[35,36] T2*-weighted anatomical images were used to drive all registration steps. Before registration, anatomical images were skull-stripped using an automated algorithm based on intensity thresholding and morphologic operations. Skull-stripped images were registered via affine transformation followed by a multiresolution, iterative, greedy symmetric normalization (SyN) non-linear registration. An average template was constructed from the sham control group using a minimum deformation template (MDT) strategy, which uses pairwise, non-linear image registrations to construct an unbiased template needing the minimum amount of deformation from each of the starting points.[37] The MDT algorithm was implemented in Linux shell script using ANTs as the registration program. This initial template construction step yields bidirectional transforms between each sham control individual and the template space. The two treatment groups were then spatially normalized to the average sham control template using a similar registration algorithm. In all cases, the similarity metric used for registration was cross-correlation computed for a kernel radius of 4 voxels. The algorithm converged at each step of the registration. The resultant transformations were applied directly to DTI-derived scalar images (described in the next section) to create population averages and were applied to tensor volumes using log-Euclidean math operations to create average tensors for tractography.[38]

### *Voxelwise analysis of diffusion tensor parameters*

After image registration, voxelwise comparisons of diffusion tensor parameters were carried out in MATLAB using the SurfStat voxelwise analysis toolkit (http://www.math.mcgill.ca/keith/surfstat/). We analyzed differences in four parameters between the sham control and treatment groups: MD, axial diffusivity (AD), radial diffusivity (RD), and FA. All image data were spatially smoothed before voxelwise analysis using a $3 \times 3 \times 3$ voxel smoothing kernel to correct for minor misregistrations. We tested for statistically significant voxels across a whole-brain mask that had undergone morphologic erosion to avoid false positives on the surface of the brain resulting from imperfect skull-stripping. Multiple comparison correction was achieved with using the false discovery rate (FDR) algorithm with a significance threshold of $q < 0.05$ (referred to as the ''adjusted $p$ value'' hereafter). Significant clusters smaller than 100 voxels were excluded from the analysis.

### *Tractography-based analysis*

To further focus our results, we tested for voxelwise statistical significance across a white matter region of interest (ROI) defined by diffusion tractography. We performed whole-brain tractography on the sham control group average tensor using an FA threshold of 0.25, a turning angle threshold of 45 degrees, and a length threshold of 1 mm. These tracking parameters were chosen based on previous experience with similar data and are consistent with those used in a recently published DTI atlas of the adult rat brain.[39] Tractography-based voxelwise analysis was performed on all voxels containing three or more tractography streamlines. Once again, we chose a significance threshold of adjusted $p < 0.05$ after FDR correction for multiple comparisons.

### *Histotechnical procedures*

After imaging, fixed brains were removed from the heads and postfixed in the same fixative solution for 6 h at 4°C. After cryoprotection in 0.1 M phosphate buffer (pH 7.4) containing 20% sucrose for 72 h at 4°C, brains were rapidly frozen and stored at −80°C. Serial sections of 40 $\mu$m thickness were cut on a cryostat coronally through the cerebrum, the brainstem, and the cerebellum, approximately from bregma 0.00 mm to −12.48 mm.[40] Every tenth section (interval: 400 $\mu$m) was collected separately in FD section storage solution™ (FD NeuroTechnologies) and stored at −20°C before further processing. Sections were processed for the detection of neurodegeneration with de Olmos amino-cupric-silver technique, which is described in detail elsewhere.[13,41] After silver staining, sections were washed thoroughly in distilled water, mounted on gelatin-coated slides, and counterstained with FD Neutral red solution™ (FD NeuroTechnologies). After dehydration in ethanol and clearing in xylene, sections were coverslipped with Permount® (Fisher Scientific, Fair Lawn, NJ).

### *Histopathologic evaluations*

There were 30 coronal sections of the brain for each of the 26 animals included in this component of the study (i.e., 10 slides with three sections/slide for each rat). The most rostral section was at the

level of the optic chiasm and/or anterior commissure, and the most caudal at the level of the deep cerebellar nuclei. All sections were examined in non-blinded fashion by a neuropathologist. Note that a non-blinded approach is most appropriate for microscopic evaluations in this type of study, because this allows for periodic comparisons of the patterns of silver staining in both control and experimental animals. Microscopic findings were subjectively graded on a five-tiered scale (minimal to marked) and recorded for 44 representative neuroanatomic regions using a PC-based histopathology program (GLPath™).

## Results

### *Experimental design and air blast exposure*

Three experimental groups were used to study the effects of repetitive primary blast overpressure exposure: a sham control group, a single blast exposed group, and a double blast exposed group (Fig. 1). All three experimental groups consisted of nine animals each. The sham control group was only exposed to inhalation anesthesia and handling without blast overpressure exposure.

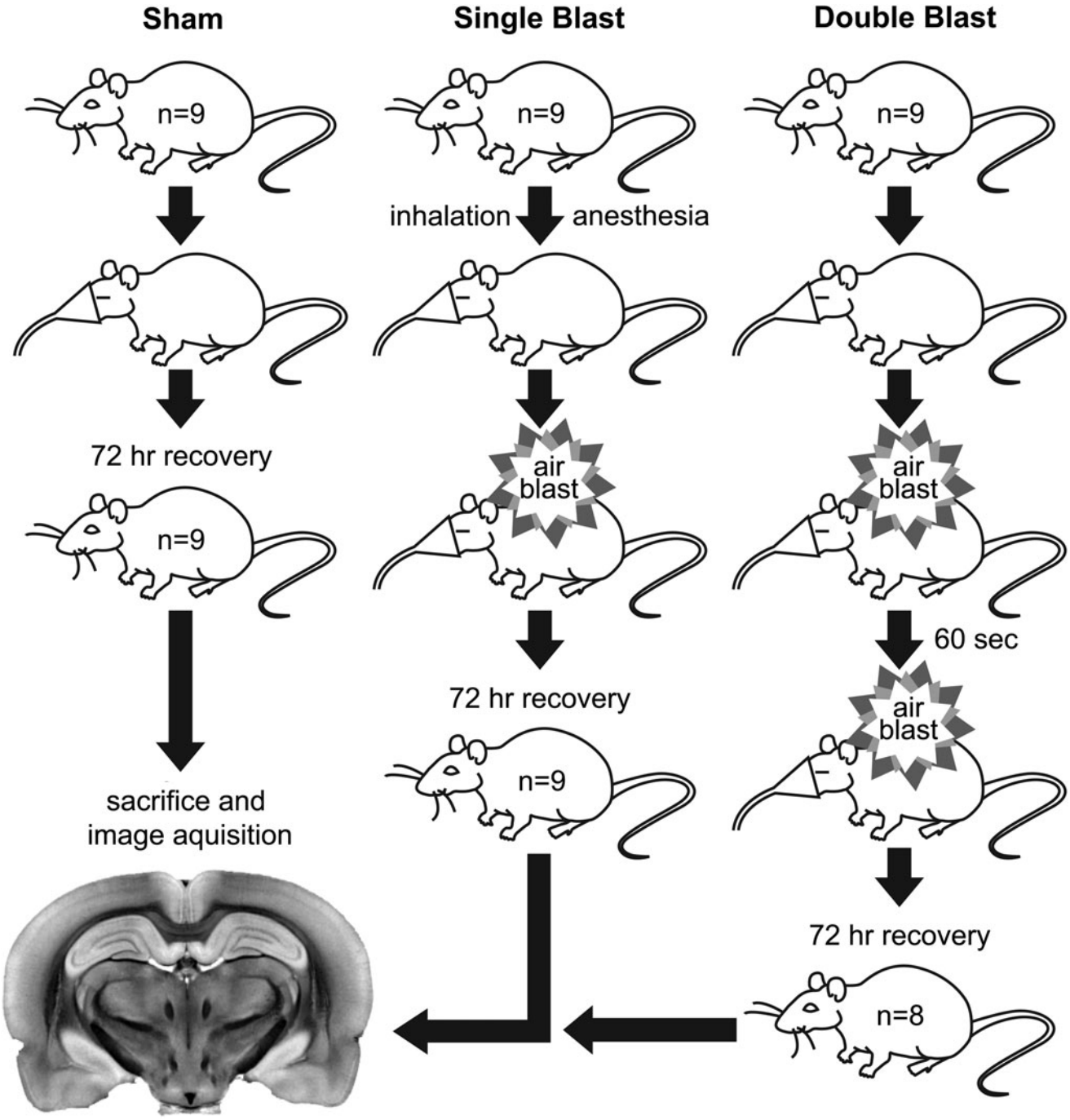


**FIG. 1.** Experimental design. There were three experimental groups: sham control, single blast, and double blast, each with $n = 9$. All animals were deeply anesthetized with inhalation anesthesia. Animals in the single blast group were exposed to a single air blast. Animals in the double blast group were exposed to two air blasts 60 sec apart. After a 72-h recovery period, animals were euthanized and imaged. A single animal in the double blast group died after exposure and was not imaged.

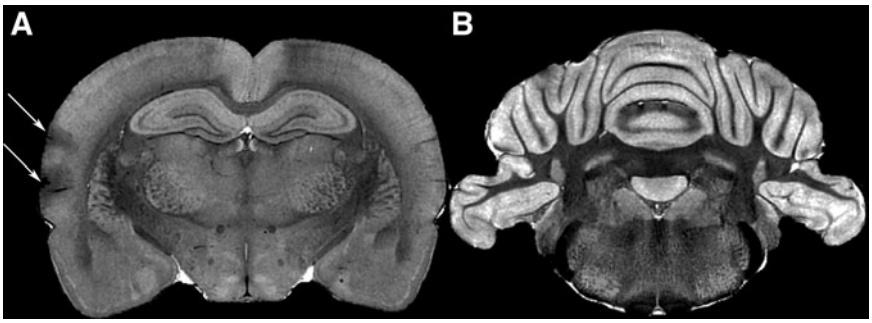


**FIG. 2.** Representative anatomical image data from a double blast exposed animal. Coronal slices through the dorsal hippocampus (**A**) and the deep cerebellar nuclei (**B**) are shown. Five of eight double blast exposed animals had cortical contusions of varying sizes, with and without associated subdural hemorrhage (arrows). No gross pathology was visible in the cerebellar white matter.

The single blast group was exposed to a single air blast. The double blast group was exposed to two air blasts temporally separated by 60 sec. All three groups received anesthesia for approximately the same period. No external injuries were observed in any of the experimental animals; however, one animal in the double blast group died shortly after exposure and was not imaged. After a 72-h recovery and observation period, rats were euthanized and prepared for imaging.

### *Anatomic image data*

High resolution T2*-weighted anatomical images from all three groups were examined for gross pathological changes (Fig. 2). No gross pathology was visible in anatomical images from either the sham control or single blast group; however, several specimens in the double blast group had prominent cortical contusions (indicated in Fig. 2 with white arrows) with and without subdural hemorrhage. Contusions were observed in five of the eight brains from the double blast group, principally located in the auditory and secondary somatosensory cortical areas. The remaining three double blast exposed brains had no visible cortical pathology. No gross pathology was observed in the cerebellar white matter or other major white matter structure in any of the three experimental groups. Complete anatomic image data from all three groups are available from the Duke University Center for In Vivo Microscopy.

### *DTI data*

FA images were also examined for gross pathology (Fig. 3). DTI-derived images like FA, although lower resolution, can be more sensitive for detecting neuropathology than anatomical images. FA images from all three groups were qualitatively very similar; however, subtle FA differences between groups were noted in the cerebellar white matter (indicated in Fig. 3 with white arrows). Both blast exposed groups appeared to have lower FA values in the cerebellar white matter than sham control animals, and this effect was more pronounced in the double blast group. Qualitative differences in other DTI-derived images were difficult to appreciate. Complete tensor volumes from all three groups are available from the Duke University Center for In Vivo Microscopy at http://www.civm.duhs.duke.edu/rat_btbi/.

### *Whole-brain voxelwise analysis*

Voxelwise analysis was used to test for statistically significant differences in DTI-derived images between the three experimental groups. No statistically significant differences were found in MD or AD, and these results are not included here. The results of the FA and RD comparisons are shown in Figures 4 and 5. Voxelwise analysis results were visualized both in 3D (Fig. 4) and as two-dimensional color overlays on anatomical images (Fig. 5). Videos of statistically significant voxel clusters rotating in 3D to allow

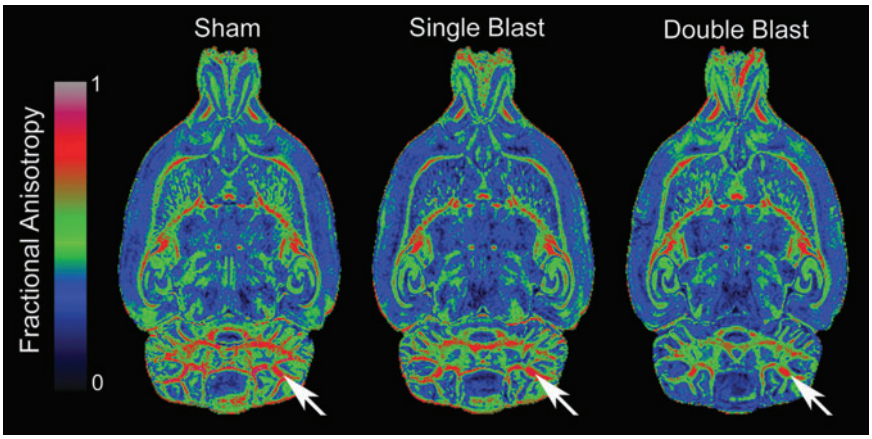


**FIG. 3.** Representative fractional anisotropy (FA) maps from all three experimental groups. Horizontal FA images through the dorsoventral center of the cerebellar white matter are displayed with a heat-map lookup table (see legend) to highlight differences. FA differences between groups are apparent in the cerebellar white matter (arrows). Color image is available online at www.liebertpub.com/neu

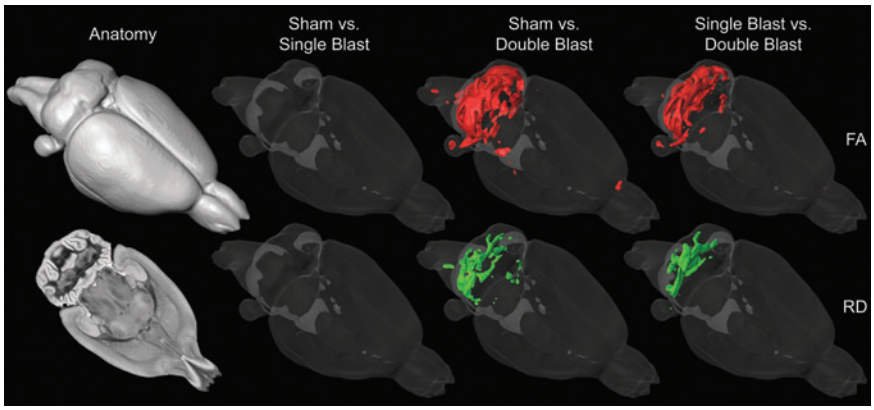


**FIG. 4.** Three-dimensional (3D) maps of statistically significant differences in diffusion tensor imaging parameters between all three experimental groups. Voxel clusters with an adjusted *p* value less than 0.05 are displayed as 3D, colored surfaces within a transparent surface rendering of the entire brain. Statistically significant differences in fractional anisotropy (red) and radial diffusivity (green) are shown for each pair of experimental groups. The left-most column contains anatomical references including an opaque surface rendering of the entire brain (top) and a single horizontal slice of the average anatomical image volume (bottom). Color image is available online at www.liebertpub.com/neu

visualization of the full 3D extent of the detected injury are available from the Duke University Center for In Vivo Microscopy at http://www.civm.duhs.duke.edu/rat_btbi/.

There were no statistically significant differences between sham control and single blast groups; however, there were small decreases in FA and increases in RD in the cerebellar white matter and axial hindbrain (Fig. 5, left).

The sham versus double blast comparison (Fig. 5, middle) revealed extensive and highly significant decreases in FA throughout the cerebellar white matter tree and cerebellar peduncles. The

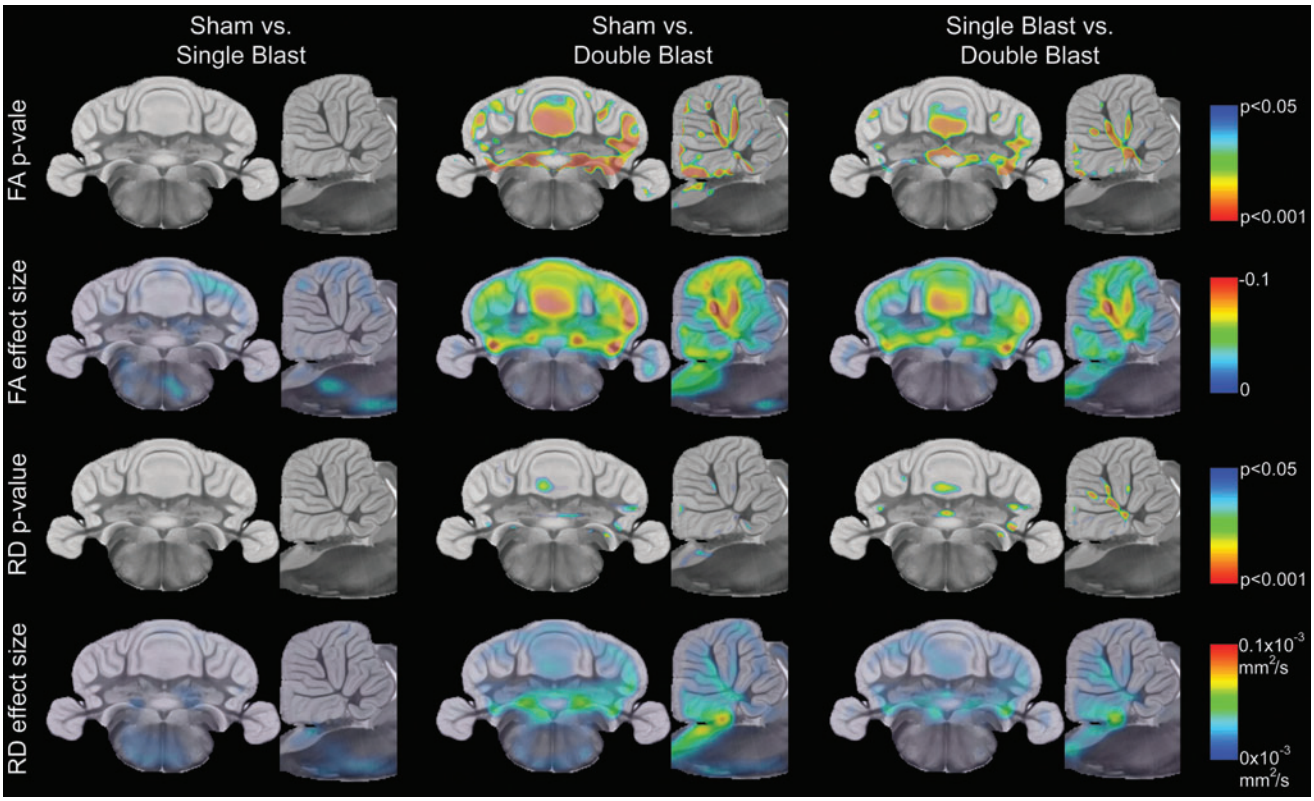


**FIG. 5.** Statistical significance and effect size maps of diffusion tensor imaging parameter differences between all three experimental groups. Adjusted *p* value maps (rows one and three) indicate statistically significant differences (adjusted *p* value less than 0.05) with color; hotter colors indicate increased confidence. Effect size maps (rows two and four) are shown across the entire brain irrespective of significance with hotter colors indicating increased effect size. FA, fractional anisotropy; RD, radial diffusivity. Color image is available online at www.liebertpub.com/neu

measured effect size in statistically significant areas was generally close to $-0.1$ arbitrary units. There were also several small regions of statistically significant increase in RD in cerebellar white matter in the sham versus double blast comparison, with effect size ranging from $5\times10^{-5}$ mm$^2$/sec to $1\times10^{-4}$ mm$^2$/sec. There was a particularly large RD increase ($\approx 1\times10^{-4}$ mm$^2$/sec) in the dorsal hindbrain, a small portion of which reached statistical significance.

The results of the single blast versus double blast (Fig. 5, right) were quite similar to those of the sham versus double blast comparison. Statistically significant decreases in FA were detected in the same regions, although to a lesser spatial extent and magnitude. Statistically significant increases in RD were actually slightly more extensive in the single blast versus double blast comparison, although the effect size was smaller.

There are a few areas in which statistical significance maps appear to extend from white matter tracts to adjacent gray matter areas (e.g., Fig. 5, center). These areas of apparent gray matter significance could be: (1) false positives from residual misregistrations between groups, (2) true positive differences in gray matter structures, or (3) blurring of true positive results in white matter caused by the spatial smoothing kernel used during voxelwise analysis preprocessing.

### *Tractography-based analysis*

Tractography-based analysis was used to focus statistical comparisons with white matter, thereby excluding a large number of gray matter voxels where blast injury is not expected. This

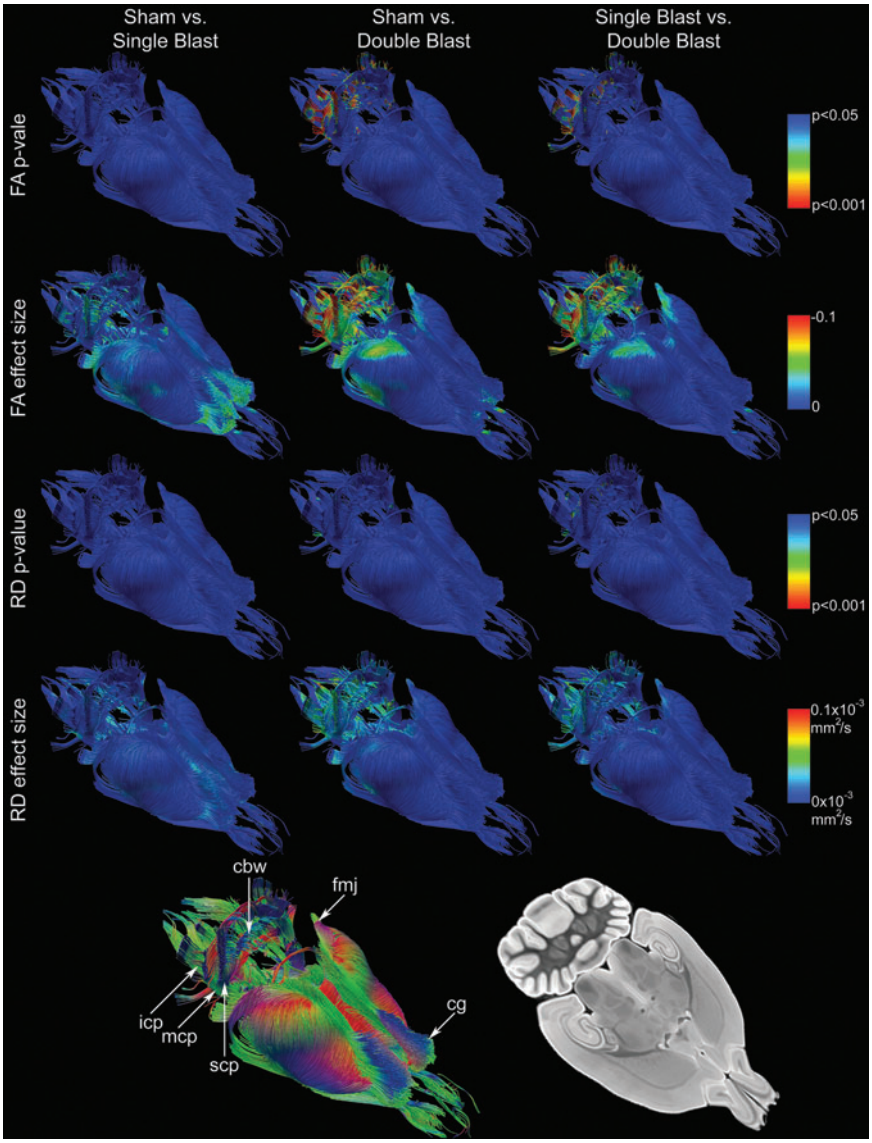


**FIG. 6.** Tractography-based analysis of diffusion tensor parameter differences between all three experimental groups. Statistical significance and effect size for each comparison (columns) are shown as colored tractography streamlines with hotter colors indicating increased statistical certainty (adjusted *p* value maps) or increased effect size (effect size maps). Anatomical references are included at the bottom of the figure including directionally colored tractography streamlines (left) and a horizontal slice of the anatomical image volume (right). Labeled structures are: cerebellar white matter (cbw); forceps major of the corpus callosum (fmj); cingulum bundle (cg); inferior, middle and superior cerebellar peduncles (icp, mcp, and scp respectively). FA, fractional anisotropy; RD, radial diffusivity. Color image is available online at www.liebertpub.com/neu

technique also allows 3D visualization of affected white matter tracts (Fig. 6). Once again, we were unable to detect statistically significant differences between sham and single blast groups; however, we did observe small decreases in FA ($\approx 0.04$ arbitrary units) in the rostral cingulum bundle and the cerebellar white matter (Fig. 6, left). Modest increases in RD ($\approx 3 \times 10^{-5}$ mm$^2$/sec) were observed in the same regions.

The sham versus double blast comparison (Fig. 6, center) yielded the most robust differences; FA was reduced throughout the cerebellum and hindbrain, and small decreases extended anteriorly as far as the caudal forceps major of the corpus callosum. FA decreases achieved statistical significance throughout the deep cerebellar white matter and in the inferior, middle, and superior cerebellar peduncles. RD increases were present in the cerebellar white matter and in all three cerebellar peduncles; however, only a limited number of tracts in the cerebellar white matter and middle cerebellar peduncle survived FDR multiple comparison correction.

The single blast versus double blast comparison (Fig. 6, right) once again revealed similar, although less extensive and lower magnitude differences than the sham versus double blast comparison. Statistically significant decreases in FA were most prominent in the cerebellar white matter and the inferior cerebellar peduncle and statistically significant increases in RD were limited to the cerebellar white matter. High-definition videos of tractography-based analysis results rotating in 3D are available from the Duke University Center for In Vivo Microscopy.

### *Silver stained histology*

Silver stained histology was used to validate voxelwise analysis findings because FA and RD, although sensitive, are not specific for white matter injury. Representative histology results are shown in Figure 7. In histology sections stained with amino cupric silver, damaged neurons and neuronal processes stain black and often take on a fragmented appearance. The sham control group in this study did not show significant silver staining anywhere in the brain. Silver staining in blast exposed animals was divided into patterns suggestive of neuronal degeneration and/or diffuse axonal injury. No degenerating neurons were present in the single blast group; however, 3/8 animals in the double blast group showed evidence of mild to moderate neuron degeneration in various regions of the cortex (*viz* frontal, parietal, temporal, and occipital).

Axonal staining in a pattern suggestive of diffuse axonal injury was more prominent than neuron degeneration. In both the single and double blast groups, the cerebellar white matter, optic tracts, and cerebellar peduncles were most commonly affected (Fig. 7). Specifically, the cerebellar white matter was affected in 8/9 rats in the single blast group (average severity = mild) versus 8/8 rats in the double blast group (average severity = moderate). The optic tracts were affected in 6/9 rats in the single blast group (average severity = mild) versus 8/8 rats in the double blast group (average severity = moderate). The cerebellar peduncles were affected in 6/9 rats in the single blast group (average severity = minimal) versus 8/8 rats in the double blast group (average severity = mild). No other neuroanatomical regions showed significant degrees of axonal damage in the single blast group. Some brains in the double blast group, however, also had evidence of axonal injury within the spinal trigeminal tract (7/8), midbrain (3/8), cochlear nucleus/nerve (3/8), and within the third and/or fourth cranial nerves (4/8).

Overall perfusion fixation was very effective at flushing the cerebral vasculature of blood; however, clotted blood was observed in the subdural space of several specimens with prominent cortical contusions. This iron-laden clotted blood could affect MRI results through susceptibility artifacts, but these effects would likely be limited to the cortical surface.

## Discussion

### *Air-blast exposure*

The blast overpressure exposure used in this study and more thoroughly characterized elsewhere[42,43] reproducibly recreates

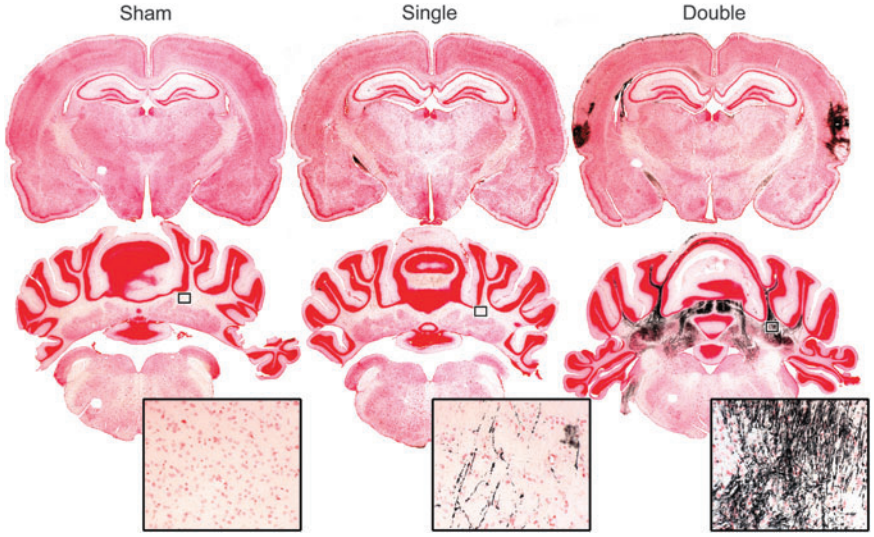


**FIG. 7.** Representative silver degeneration-stained coronal brain sections from all three experimental groups: sham control (left) single blast exposed (center) and double blast exposed (right). Two coronal sections are shown for each group—one at the level of the dorsal hippocampus at approximately Bregma −3.3 mm (top), and one through the cerebellum at approximately Bregma −11.4 mm (bottom). Magnified insets are medium-high power micrographs (20× objective) of the cerebellar white matter showing silver staining of axons and the formation of axon retraction balls typical of those seen in traumatic axonal injury. Color image is available online at www.liebertpub.com/neu

with some fidelity the primary blast pressure wave created by explosive detonations. Unfortunately, comparing experimental blast conditions with combat-related blast exposure is difficult because of the intrinsic limitations of the shock tube model, as well as significant anatomical and physiological differences between humans and rodents. Nonetheless, similar experimental conditions are widely used to study the effects of blast overpressure in small animal models. This exposure technique provides the opportunity to study the effects of a realistic primary blast pressure wave in the absence of concomitant secondary or tertiary blast injury. Blast wind-induced head acceleration has recently received attention as a primary injury mechanism contributing to experimental blast-related TBI[44]; however, in the present study, these contributions have been minimized by secure immobilization of each subject in the holder during blast overpressure exposure. Previous histological assessment of this model has shown extensive axonal damage in several major white matter tracts, most notably the cerebellar white matter.[17] These histological findings, coupled with impaired performance in motor tasks, correlate well with some injuries and symptoms seen in clinical populations.[10,18,29]

We chose to study the effects of repeated blast exposure based on previous experimental and clinical observations that repeated head injuries can cause cumulative or even synergistic neurological damage.[45,46] The rationale for administering blast exposures 1 min apart was based on previous observations in mice, in which greatly exacerbated mortality, neuropathological changes, and neurobehavioral disruptions were noted with blast exposures separated by 1 and 30 min.[17] In future studies, this model will allow characterization of the window of vulnerability to a second blast exposure.

### *Anatomic image data*

The anatomical image data presented in Figure 2 highlights the difficulty in traditional image-based assessment of bTBI. Anatomical imaging yielded inconsistent results that did not correlate well with DTI findings. The only grossly visible lesions were cortical contusions of varying severity with or without subdural hemorrhage in five of the eight double-blasted specimens. These imaging findings are quite similar to those seen in clinical populations where cortical contusions and subdural hemorrhages are among the most commonly observed lesions.[47] Interestingly, our results suggest that these lesions, which are often associated with cortical impact and/or acceleration/deceleration injury, can result from primary blast pressure wave exposure alone. There were no grossly evident lesions in the cerebellum or hindbrain despite these being the primary sites of axonal injury as detected by voxelwise analysis of DTI parameters. These results highlight the need for advanced imaging and computational approaches to assess occult microstructural injury in bTBI. It is possible that grossly visible lesions resulting from bTBI are merely the ''tip of the iceberg'' indicating more extensive and possibly more clinically relevant occult white matter injury.

### *DTI parameter data*

Diffusion tensor parameters, such as FA and RD, have garnered attention as highly sensitive, yet non-specific, markers of white matter microstructural integrity. These quantitative parameters, which are based on the microscopic diffusion properties of water, have the potential to reveal microstructural damage at a scale that is much smaller than the voxel size of the image itself.[26] For example, axonal injury causes decreases in FA, often accompanied by increases in RD, although many other microstructural changes, such as edema and gliosis, can produce similar findings.[27] We observed subtle, although grossly visible decreases in FA in the cerebellum that were more severe in the double blast group than the single blast group (Fig. 3). Unfortunately, these differences are small, and it is difficult to appreciate their full spatial extent from simple, ROI-based image comparisons.

### *Pitfalls of voxelwise analysis*

Voxelwise analysis of DTI parameters is a powerful investigational technique that allows researchers to test for significant differences across the entire brain without predefined anatomical hypotheses. Unfortunately, voxelwise analysis is vulnerable to a number of pitfalls that can lead to false positive results. Two of the most common causes of false positive results are minor misregistrations between treated and control groups, and failure to correct for multiple comparisons.[48,49] In this study, we have taken a number of steps to ensure accurate registration including the use of: (1) high-resolution, high-SNR diffusion-weighted images, (2) an unbiased MDT registration strategy, and (3) registration software specifically optimized for small animal image data. To correct for any residual misregistrations, images were spatially smoothed with a three-voxel 3D Gaussian kernel consistent with general guidelines for voxelwise analysis.[49,50] Multiple comparison correction was achieved using the FDR method, which is less stringent than family wise error rate methods, but more robust than arbitrarily defined *p*-thresholds. We have used this cautious methodology to identify only the most robust and reproducible injuries resulting from primary blast exposure, because these are likely to be the most meaningful targets for intervention.

### *Voxelwise analysis of repeated primary blast exposure*

The results of our voxelwise analysis show a consistent pattern of injury to the major cerebellar white matter tracts in double blast exposed animals. These areas show FA loss concomitant with RD increase—a pattern that is frequently observed in traumatic axonal injury.[51,52] Interestingly, we observed no statistically significant differences in AD, suggesting that RD increases are the primary cause of anisotropy loss in affected areas. AD decrease is also a common finding in acute axonal injury, although it often normalizes in the sub-acute and chronic setting.[51,53] It is possible that AD decreases are not a major feature of primary bTBI or that the changes are too small and/or variable to detect using our methods. In addition, the DTI parameter changes that we observed are likely only present in the acute to sub-acute (i.e., $< 72$ h) post-injury period. Assessment of later post-injury time points may reveal completely different DTI parameter changes driven by edema, necrosis, and/or gliosis.

We were unable to detect any statistically significant differences between single blast and sham control groups; however, there were large and highly significant differences between the single blast and double blast groups. By all imaging metrics, the single blast group more closely resembled the sham control group than the double blast group. This result suggests a synergistic effect with repeated blast exposure. One possible explanation is that initial blast exposure sensitizes the brain, either physiologically or mechanically, to damage from a subsequent blast. Several physiological changes are known to occur immediately after closed head injury in animal models, including increases in heart rate, arterial blood pressure, and intracranial pressure.[54,55] Each of these parameters could potentially magnify subsequent blast injury by altering the

intracranial fluid pressure dynamics that are thought to underlie primary blast wave associated injury.[7,56] Mechanical sensitization could occur by weakening or degradation of the neuronal cytoskeleton, which has also been observed in rodent models of primary bTBI.[57,58] Further studies are needed to determine what, if any, are the mechanisms of sensitization to further injury. For example, real-time monitoring of intracranial and intravascular pressures during repeated blast exposure could elucidate the role of pressure dynamics, and immunofluorescence or electron microscopy studies could be used to assess cytoskeletal injury. Because DTI is non-destructive, it can easily be combined and correlated with higher resolution imaging techniques such as electron microscopy.[22]

### *Tractography-based analysis*

Tractography-based analysis is a special case of voxelwise analysis that is well suited for detection and visualization of white matter injury.[59] Applying tractography-based analysis to this study is justified based on a number of previous studies suggesting that primary bTBI is predominantly a white matter injury.[6,9,10,29] Tractography-based analysis has two main advantages over whole-brain voxelwise analysis. First, it provides more focused and potentially less biased results by limiting the analysis to a white matter skeleton defined by the control group average tractography streamlines.[60,61] Second, it permits 3D visualization of significance and effect size maps through the use of color-coded tractography streamlines.

The tractography-based analysis presented here allowed precise localization of blast-induced white matter injury to the cerebellar white matter and cerebellar peduncles. Tractography-based results also highlight the dramatic differences between single blast and double blast-associated injury. The second blast dramatically increased both the spatial extent and the magnitude of the associated white matter injury. Together, these results suggest that specific subtentorial white matter tracts, like the cerebellar white matter, may be uniquely susceptible to repeated primary bTBI. Interestingly, similar injury patterns have been reported in both clinical populations[6,10,29] and in previous animal studies.[13,16,17] Further, hindbrain white matter injury is consistent with several common symptoms of bTBI including tinnitus, vertigo, and balance/motor-coordination problems. Previously published behavioral assessments of the blast injury model used in this study have demonstrated impaired performance on standardized motor coordination tests such as beam walking and the Morris water maze.[15] Future studies are needed to explore the correlation between motor task performance and cerebellar white matter injury as detected by DTI.

### *Histological validation of voxelwise analysis results*

The results of our histological examination of neuronal injury correlate well with voxelwise analysis results, both in spatial extent and in magnitude. Silver staining revealed modest and inconsistent axonal injury in the cerebellar white matter of single blasted brains. This low magnitude and highly variable injury explains why DTI parameter changes did not reach statistical significance for the single blast versus sham control comparison. In contrast, histological examination of double blasted brains revealed severe and consistent axonal injury within the cerebellar white matter tree. These results closely match the statistically significant regions of RD decrease and FA increase detected with voxelwise analysis of the double blast group.

Comparison of histology results with DTI voxelwise analysis results demonstrates the benefits and drawbacks of each technique. Silver stained histology is far more sensitive and can detect injury as small as a single damaged neuron. DTI has neither the spatial resolution nor the sensitivity to detect such small-scale damage; however, DTI has several major advantages over histology. First, DTI is 3D and non-destructive, so pathology can be detected throughout the entire brain without distortion or sectioning artifact. Second, DTI parameters allow straightforward quantitative comparisons, and voxelwise analysis techniques can be used to test for statistically significant differences throughout the entire brain without an *a priori* anatomical hypothesis. Although quantitative analysis of histology is possible, it is often technically difficult, time consuming, limited to predefined anatomical regions, and/or non-parametric. Nonetheless, quantitative histology is the *de facto* gold standard for assessing neuropathological alterations resulting from blast injury, as is evident from a large body of previously published work. Although the current study is focused on quantitative assessment of DTI rather than histology, a comparison of both quantitative techniques will undoubtedly be an important area of future work. Finally, although the present study uses fixed *ex vivo* specimens, voxelwise analysis of DTI parameters is possible *in vivo* and may even be more sensitive for detecting differences in living subjects.[62]

### *Limitations of this study*

This study has several important limitations. First, the rat may not be the ideal model system for studying human brain injury.[63] Non-human primate models may more closely recapitulate human bTBI; however, ethical and technical considerations make rodent models much more desirable. Further, a large body of previous research supports the use of rodents for studying human bTBI. Second, both death and tissue fixation are known to affect diffusion tensor parameter measurements, which is an important consideration for *ex vivo* studies. Formalin fixation is known to reduce tissue diffusivity; however, it appears to do so both proportionally and uniformly throughout the brain, thus preserving anisotropy.[64] As a result, the relative RD differences that we report likely reflect *in vivo* changes, but the absolute magnitudes do not. Importantly, fixation also seems to reduce the sensitivity of DTI in detecting axonal damage, suggesting a comparable *in vivo* study may be able to detect even more subtle injury.[62] Nevertheless, *ex vivo* imaging has several important benefits including higher SNR and higher spatial resolution.[65] Finally, there is considerable debate over the proper acquisition protocol for measuring diffusion tensor parameters, with some studies recommending as many as 30 gradient directions[66,67]; however, these studies are based on clinical data where patient movement, low SNR, and susceptibility artifacts are major sources of error. Any error resulting from a six-direction strategy is, to some extent, compensated for by the increased image quality, SNR, and spatial accuracy that *ex vivo* DTI can provide.[68,69]

## Conclusions

This work contributes to the growing body of data suggesting that primary blast injury is an important component of bTBI. Further, we provide preclinical evidence that brain injury increases synergistically with repeated exposure to blast overpressure. Our results suggest that the primary blast wave sensitizes the brain to more severe injury from subsequent blast exposure, even in the absence of radiologically detectable gross pathology. This

conclusion, if supported by further studies, has widespread significance for the treatment of soldiers subjected to blasts in the battlefield, many of whom remain on active duty after exposure. A critical area of future research will be to determine the time-course of primary bTBI associated sensitization to further brain injury. For example, if the observed sensitization effect is related to intravascular and/or intracranial pressure dynamics, then it may only persist for minutes to hours until equilibrium is restored. Conversely, if sensitization is caused by cytoskeletal damage, then it would be expected to persist for hours to days until repair completes. A follow-up study with varying time intervals between blasts will be important in understanding both the underlying mechanism of sensitization and the implications for human bTBI patients.

The methods and model system described here have exciting potential to further our understanding of the effects of the primary blast wave on the brain. Voxelwise analysis of DTI parameters has proven to be a useful and sensitive tool for detecting primary bTBI in rodent models and is readily translatable to human studies. We look forward to using similar techniques to study not only the time-course of primary bTBI, but also its interaction with other forms of blast injury. Unfortunately, combat-related bTBI usually involves acceleration/deceleration and/or cranial impact injuries, which may have complex interactions with primary blast injury. These interactions could be explored using a combination of shock tube blast overpressure and other rodent TBI models such as weight-drop contusion or controlled cortical impact. Although such studies present a significant logistical challenge, they may ultimately prove to be more clinically relevant than the repetitive injury model presented here. Finally, we would like to reiterate that all image data, including full tensor volumes, are available from the Duke University Center for In Vivo Microscopy. We welcome and encourage further analysis, because we are confident there is still more valuable information to be extracted from this dataset.

## Acknowledgments

The views, opinions, and/or findings contained herein are those of the authors and should not be construed as an official position, policy, or decision of the Department of the Army or the Department of Defense.

Animal handling and treatments were conducted in compliance with the Animal Welfare Act and other Federal statutes and regulations related to animals and experiments involving animals, and adhered to principles stated in the Guide to the Care and Use of Laboratory Animals, National Research Council. The facilities are fully accredited by the Association for Assessment and Accreditation of Laboratory Animal Care International.

Blast exposure was performed at the Walter Reed Army Institute of Research under the support of the CDMRP Psychological Health and Traumatic Brain Injury Research Program (W81XWH-11-2-0127). Imaging work was performed at the Duke University Center for In Vivo Microscopy, an NIH/NIBIB Biomedical Technology Resource Center (P41 EB015897). We are grateful to Sally Gewalt and James Cook for assistance with the imaging pipelines. We thank Andrea Edwards, Joseph Andrist, and Donna Wilder for assistance with blast exposures, and Dr. Yi Qi, and Gary Cofer for assistance in specimen preparation and scanning.

## Author Disclosure Statement

No competing financial interests exist.

## References

1. Hoge, C.W., McGurk, D., Thomas, J.L., Cox, A.L., Engel, C.C., and Castro, C.A. (2008). Mild traumatic brain injury in U.S. Soldiers returning from Iraq. N. Engl. J. Med. 358, 453–463.
2. Warden, D. (2006). Military TBI during the Iraq and Afghanistan wars. J. Head Trauma Rehabil. 21, 398–402.
3. Okie, S. (2005). Traumatic brain injury in the war zone. N. Engl. J. Med. 352, 2043–2047.
4. Schneiderman, A I., Braver, E.R., and Kang, H.K. (2008). Understanding sequelae of injury mechanisms and mild traumatic brain injury incurred during the conflicts in Iraq and Afghanistan: persistent postconcussive symptoms and posttraumatic stress disorder. Am. J. Epidemiol. 167, 1446–1452.
5. DeKosky, S.T., Ikonomovic, M.D., and Gandy, S. (2010). Traumatic brain injury—football, warfare, and long-term effects. N. Engl. J. Med. 363, 1293–1296.
6. Mac Donald, C.L., Johnson, A.M., Cooper, D., Nelson, E.C., Werner, N.J., Shimony, J.S., Snyder, A.Z., Raichle, M.E., Witherow, J.R., Fang, R., Flaherty, S.F., and Brody, D.L. (2011). Detection of blast-related traumatic brain injury in U.S. military personnel. N. Engl. J. Med. 364, 2091–2100.
7. Taylor, P.A., and Ford, C.C. (2009). Simulation of blast-induced early-time intracranial wave physics leading to traumatic brain injury. J. Biomech. Eng. 131, 061007.
8. Cernak, I., and Noble-Haeusslein, L J. (2010). Traumatic brain injury: an overview of pathobiology with emphasis on military populations. J. Cereb. Blood Flow Metab. 30, 255–266.
9. Hayes, J.P., Morey, R.A., and Tupler, L.A. (2012). A case of frontal neuropsychological and neuroimaging signs following multiple primary-blast exposure. Neurocase 18, 258–269.
10. Warden, D.L., French, L.M., Shupenko, L., Fargus, J., Riedy, G., Erickson, M.E., Jaffee, M.S., and Moore, D.F. (2009). Case report of a soldier with primary blast brain injury. Neuroimage 47, Suppl 2, T152–T153.
11. Sylvia, F.R., Drake, A.I., and Wester, D.C. (2001). Transient vestibular balance dysfunction after primary blast injury. Mil. Med. 166, 918–920.
12. Rubovitch, V., Ten-Bosch, M., Zohar, O., Harrison, C.R., Tempel-Brami, C., Stein, E., Hoffer, B.J., Balaban, C.D., Schreiber, S., Chiu, W.T., and Pick, C.G. (2011). A mouse model of blast-induced mild traumatic brain injury. Exp. Neurol. 232, 280–289.
13. Garman, R.H., Jenkins, L.W., Switzer, R.C. III, Bauman, R.A., Tong, L.C., Swauger, P.V., Parks, S., Ritzel, D.V., Dixon, C.E., Clark, R., Bayir, H., Kagan, V., Jackson, E., and Kochanek, P.M. (2011). Blast exposure in rats with body shielding is characterized primarily by diffuse axonal injury. J. Neurotrauma 28, 947–959.
14. Mao, J.C., Pace, E., Pierozynski, P., Kou, Z., Shen, Y., Vandevord, P., Haacke, E.M., Zhang, X., and Zhang, J. (2012). Blast-induced tinnitus and hearing loss in rats: behavioral and imaging assays. J. Neurotrauma 29, 430–444.
15. Long, J.B., Bentley, T.L., Wessner, K.A., Cerone, C., Sweeney, S., and Bauman, R.A. (2009). Blast overpressure in rats: recreating a battlefield injury in the laboratory. J. Neurotrauma 26, 827–840.
16. Bauman, R.A., Ling, G., Tong, L., Januszkiewicz, A., Agoston, D., Delanerolle, N., Kim, Y., Ritzel, D., Bell, R., Ecklund, J., Armonda, R., Bandak, F., and Parks, S. (2009). An introductory characterization of a combat-casualty-care relevant swine model of closed head injury resulting from exposure to explosive blast. J. Neurotrauma 26, 841–860.
17. Wang, Y., Wei, Y., Oguntayo, S., Wilkins, W., Arun, P., Valiyaveettil, M., Song, J., Long, J.B., and Nambiar, M P. (2011). Tightly coupled repetitive blast-induced traumatic brain injury: development and characterization in mice. J. Neurotrauma 28, 2171–2183.
18. Peskind, E.R., Petrie, E.C., Cross, D.J., Pagulayan, K., McCraw, K., Hoff, D., Hart, K., Yu, C.E., Raskind, M.A., Cook, D.G., and Minoshima, S. (2011). Cerebrocerebellar hypometabolism associated with repetitive blast exposure mild traumatic brain injury in 12 Iraq war Veterans with persistent post-concussive symptoms. Neuroimage 54, Suppl 1, S76–S82.
19. Säljö, A., Svensson, B., Mayorga, M., Hamberger, A., and Bolouri, H. (2009). Low-level blasts raise intracranial pressure and impair cognitive function in rats. J. Neurotrauma 26, 1345–1352.
20. Mazurkiewicz-Kwilecki, I.M. (1980). Single and repeated air blast stress and brain histamine. Pharmacol. Biochem. Behav. 12, 35–39.

21. Johnson, G.A., Badea, A., and Jiang, Y. (2011). Quantitative neuromorphometry using magnetic resonance histology. Toxicol. Pathol. 39, 85–91.
22. Calabrese, E., and Johnson, G.A. (2013). Diffusion tensor magnetic resonance histology reveals microstructural changes in the developing rat brain. Neuroimage 79, 329–339.
23. Liu, C., Li, W., Johnson, G.A., and Wu, B. (2011). High-field (9.4T) MRI of brain dysmyelination by quantitative mapping of magnetic susceptibility. Neuroimage 56, 930–938.
24. Johnson, G.A., Benveniste, H., Black, R.D., Hedlund, L.W., Maronpot, R.R., and Smith, B.R. (1993). Histology by magnetic resonance microscopy. Magn. Reson. Q. 9, 1–30.
25. Johnson, G.A., Cofer, G.P., Fubara, B., Gewalt, S.L., Hedlund, L.W., and Maronpot, R.R. (2002). Magnetic resonance histology for morphologic phenotyping. J. Magn. Reson. Imaging 16, 423–429.
26. Basser, P.J. (1995). Inferring microstructural features and the physiological state of tissues from diffusion-weighted images. NMR Biomed. 8, 333–344.
27. Mukherjee, P., Berman, J.I., Chung, S.W., Hess, C.P., and Henry, R.G. (2008). Diffusion tensor MR imaging and fiber tractography: theoretic underpinnings. AJNR Am. J. Neuroradiol. 29, 632–641.
28. Sponheim, S.R., McGuire, K.A., Kang, S.S., Davenport, N.D., Aviyente, S., Bernat, E.M., and Lim, K.O. (2011). Evidence of disrupted functional connectivity in the brain after combat-related blast injury. Neuroimage 54, Suppl 1, S21–S29.
29. Mac Donald, C., Johnson, A., Cooper, D., Malone, T., Sorrell, J., Shimony, J., Parsons, M., Snyder, A., Raichle, M., Fang, R., Flaherty, S., Russell, M., and Brody, D.L. (2013). Cerebellar white matter abnormalities following primary blast injury in US military personnel. PLoS ONE 8, e55823.
30. Mac Donald, C.L., Dikranian, K., Song, S.K., Bayly, P.V., Holtzman, D.M., and Brody, D.L. (2007). Detection of traumatic axonal injury with diffusion tensor imaging in a mouse model of traumatic brain injury. Exp. Neurol. 205, 116–131.
31. Bennett, R.E., Mac Donald, C.L., and Brody, D.L. (2012). Diffusion tensor imaging detects axonal injury in a mouse model of repetitive closed-skull traumatic brain injury. Neurosci. Lett. 513, 160–165.
32. Johnson, G.A., Cofer, G.P., Gewalt, S.L., and Hedlund, L.W. (2002). Morphologic phenotyping with MR microscopy: the visible mouse. Radiology 222, 789–793.
33. Stejskal, E.O., and Tanner, J.E. (1965). Spin diffusion measurements: spin echoes in the presence of a time-dependent field gradient. J. Chem. Phys. 42, 288–292.
34. Johnson, G.A., Ali-Sharief, A., Badea, A., Brandenburg, J., Cofer, G., Fubara, B., Gewalt, S., Hedlund, L.W., and Upchurch, L. (2007). High-throughput morphologic phenotyping of the mouse brain with magnetic resonance histology. Neuroimage 37, 82–89.
35. Avants, B.B., Epstein, C.L., Grossman, M., and Gee, J.C. (2008). Symmetric diffeomorphic image registration with cross-correlation: evaluating automated labeling of elderly and neurodegenerative brain. Med. Image Anal. 12, 26–41.
36. Avants, B.B., Tustison, N.J., Song, G., Cook, P.A., Klein, A., and Gee, J.C. (2011). A reproducible evaluation of ANTs similarity metric performance in brain image registration. Neuroimage 54, 2033–2044.
37. Kochunov, P., Lancaster, J.L., Thompson, P., Woods, R., Mazziotta, J., Hardies, J., and Fox, P. (2001). Regional spatial normalization: toward an optimal target. J. Comput. Assist. Tomogr. 25, 805–816.
38. Arsigny, V., Fillard, P., Pennec, X., and Ayache, N. (2006). Log-Euclidean metrics for fast and simple calculus on diffusion tensors. Magn. Reson. Med. 56, 411–421.
39. Johnson, G.A., Calabrese, E., Badea, A., Paxinos, G., and Watson, C. (2012). A multidimensional magnetic resonance histology atlas of the Wistar rat brain. Neuroimage 62, 1848–1856.
40. Paxinos, G., and Watson, C. (2007). *The Rat Brain in Stereotaxic Coordinates.* 6th ed. Elsevier Academic Press: San Diego.
41. de Olmos, J.S., Beltramino, C.A., and de Olmos de Lorenzo, S. (1994). Use of an amino-cupric-silver technique for the detection of early and semiacute neuronal degeneration caused by neurotoxicants, hypoxia, and physical trauma. Neurotoxicol. Teratol. 16, 545–561.
42. Long, J.B., Tong, L., Bauman, R.A., Atkins, J.L., Januszkiewicz, A.J., Riccio, C., Gharavi, R., Shoge, R., Parks, S., Ritzel, D.V., and Bentley, T.B. (2010). Blast-induced traumatic brain injury: using a shock tube to recreate a battlefield injury in the laboratory. IFMBE Proc, 32, pp. 26–30.
43. Kamnaksh, A., Kovesdi, E., Kwon, S.K., Wingo, D., Ahmed, F., Grunberg, N.E., Long, J., and Agoston, D.V. (2011). Factors affecting blast traumatic brain injury. J. Neurotrauma 28, 2145–2153.
44. Goldstein, L.E., Fisher, A.M., Tagge, C.A., Zhang, X.L., Velisek, L., Sullivan, J.A., Upreti, C., Kracht, J.M., Ericsson, M., Wojnarowicz, M.W., Goletiani, C.J., Maglakelidze, G.M., Casey, N., Moncaster, J.A., Minaeva, O., Moir, R.D., Nowinski, C.J., Stern, R.A., Cantu, R.C., Geiling, J., Blusztajn, J.K., Wolozin, B.L., Ikezu, T., Stein, T.D., Budson, A.E., Kowall, N.W., Chargin, D., Sharon, A., Saman, S., Hall, G.F., Moss, W.C., Cleveland, R. O., Tanzi, R.E., Stanton, P.K., and McKee, A.C. (2012). Chronic traumatic encephalopathy in blast-exposed military veterans and a blast neurotrauma mouse model. Sci. Transl. Med. 4, 134ra60.
45. Laurer, H.L., Bareyre, F.M., Lee, V.M., Trojanowski, J.Q., Longhi, L., Hoover, R., Saatman, K.E., Raghupathi, R., Hoshino, S., Grady, M.S., and McIntosh, T.K. (2001). Mild head injury increasing the brain's vulnerability to a second concussive impact. J. Neurosurg. 95, 859–870.
46. Longhi, L., Saatman, K.E., Fujimoto, S., Raghupathi, R., Meaney, D.F., Davis, J., McMillan B. S., Conte, V., Laurer, H.L., Stein, S., Stocchetti, N., and McIntosh, T.K. (2005). Temporal window of vulnerability to repetitive experimental concussive brain injury. Neurosurgery 56, 364–374.
47. Taber, K.H., Warden, D.L., and Hurley, R.A. (2006). Blast-related traumatic brain injury: what is known? J. Neuropsychiatry Clin. Neurosci. 18, 141–145.
48. Jones, D.K., and Cercignani, M. (2010). Twenty-five pitfalls in the analysis of diffusion MRI data. NMR Biomed. 23, 803–820.
49. Abe, O., Takao, H., Gonoi, W., Sasaki, H., Murakami, M., Kabasawa, H., Kawaguchi, H., Goto, M., Yamada, H., Yamasue, H., Kasai, K., Aoki, S., and Ohtomo, K. (2010). Voxel-based analysis of the diffusion tensor. Neuroradiology 52, 699–710.
50. Jones, D.K., Symms, M.R., Cercignani, M., and Howard, R.J. (2005). The effect of filter size on VBM analyses of DT-MRI data. Neuroimage 26, 546–554.
51. Song, S.K., Sun, S.W., Ju, W.K., Lin, S.J., Cross, A.H., and Neufeld, A.H. (2003). Diffusion tensor imaging detects and differentiates axon and myelin degeneration in mouse optic nerve after retinal ischemia. Neuroimage 20, 1714–1722.
52. Newcombe, V. F., Williams, G.B., Nortje, J., Bradley, P.G., Harding, S.G., Smielewski, P., Coles, J.P., Maiya, B., Gillard, J.H., Hutchinson, P.J., Pickard, J.D., Carpenter, T.A., and Menon, D.K. (2007). Analysis of acute traumatic axonal injury using diffusion tensor imaging. Br. J. Neurosurg. 21, 340–348.
53. Sidaros, A., Engberg, A.W., Sidaros, K., Liptrot, M.G., Herning, M., Petersen, P., Paulson, O.B., Jernigan, T.L., and Rostrup, E. (2008). Diffusion tensor imaging during recovery from severe traumatic brain injury and relation to clinical outcome: a longitudinal study. Brain 131, 559–572.
54. Marmarou, A., Foda, M.A., van den Brink, W., Campbell, J., Kita, H., and Demetriadou, K. (1994). A new model of diffuse brain injury in rats. Part I: Pathophysiology and biomechanics. J. Neurosurg. 80, 291–300.
55. Rooker, S., Jorens, P.G., Van Reempts, J., Borgers, M., and Verlooy, J. (2003). Continuous measurement of intracranial pressure in awake rats after experimental closed head injury. J. Neurosci. Methods 131, 75–81.
56. Chafi, M.S., Karami, G., and Ziejewski, M. (2010). Biomechanical assessment of brain dynamic responses due to blast pressure waves. Ann. Biomed. Eng. 38, 490–504.
57. Säljö, A., Bao, F., Haglid, K. G., and Hansson, H. A. (2000). Blast exposure causes redistribution of phosphorylated neurofilament subunits in neurons of the adult rat brain. J. Neurotrauma 17, 719–726.
58. Park, E., Gottlieb, J.J., Cheung, B., Shek, P.N., and Baker, A.J. (2011). A model of low-level primary blast brain trauma results in cytoskeletal proteolysis and chronic functional impairment in the absence of lung barotrauma. J. Neurotrauma 28, 343–357.
59. Yushkevich, P.A., Zhang, H., Simon, T.J., and Gee, J.C. (2008). Structure-specific statistical mapping of white matter tracts. Neuroimage 41, 448–461.
60. Yendiki, A., Panneck, P., Srinivasan, P., Stevens, A., Zöllei, L., Augustinack, J., Wang, R., Salat, D., Ehrlich, S., Behrens, T., Jbabdi, S., Gollub, R., and Fischl, B. (2011). Automated probabilistic reconstruction of white-matter pathways in health and disease using an atlas of the underlying anatomy. Front. Neuroinform. 5, 23.

61. Goodlett, C., Davis, B., Jean, R., Gilmore, J., and Gerig, G. (2006). Improved correspondence for DTI population studies via unbiased atlas building. Med. Image Comput. Comput. Assist. Interv. 9, 260–267.
62. Sun, S.W., Liang, H.F., Xie, M., Oyoyo, U., and Lee, A. (2009). Fixation, not death, reduces sensitivity of DTI in detecting optic nerve damage. Neuroimage 44, 611–619.
63. Cenci, M.A., Whishaw, I. Q., and Schallert, T. (2002). Animal models of neurological deficits: how relevant is the rat? Nat. Rev. Neurosci. 3, 574–579.
64. Sun, S.W., Neil, J.J., Liang, H.F., He, Y.Y., Schmidt, R.E., Hsu, C.Y., and Song, S.K. (2005). Formalin fixation alters water diffusion coefficient magnitude but not anisotropy in infarcted brain. Magn. Reson. Med. 53, 1447–1451.
65. Lerch, J.P., Gazdzinski, L., Germann, J., Sled, J.G., Henkelman, R.M., and Nieman, B.J. (2012). Wanted dead or alive? The tradeoff between in-vivo versus ex-vivo MR brain imaging in the mouse. Front. Neuroinform. 6, 6.
66. Ni, H., Kavcic, V., Zhu, T., Ekholm, S., and Zhong, J. (2006). Effects of number of diffusion gradient directions on derived diffusion tensor imaging indices in human brain. AJNR Am. J. Neuroradiol. 27, 1776–1781.
67. Landman, B.A., Farrell, J.A., Jones, C.K., Smith, S.A., Prince, J.L., and Mori, S. (2007). Effects of diffusion weighting schemes on the reproducibility of DTI-derived fractional anisotropy, mean diffusivity, and principal eigenvector measurements at 1.5T. Neuroimage 36, 1123–1138.
68. Anderson, A.W. (2001). Theoretical analysis of the effects of noise on diffusion tensor imaging. Magn. Reson. Med. 46, 1174–1188.
69. Alexander, A.L., Hasan, K.M., Lazar, M., Tsuruda, J.S., and Parker, D.L. (2001). Analysis of partial volume effects in diffusion-tensor MRI. Magn. Reson. Med. 45, 770–780.

Address correspondence to:
*Joseph B. Long, PhD*
*Blast-Induced Neurotrauma Branch*
*Center for Military Psychiatry and Neuroscience*
*Walter Reed Army Institute of Research*
*Robert Grant Avenue, Building 503*
*Silver Spring, MD 20910*

*E-mail:* joseph.long@us.army.mil